Journal of Solid State Chemistry 326 (2023) 124184

Contents lists available at ScienceDirect

Journal of Solid State Chemistry

journal homepage: www.elsevier.com/locate/jssc

Structure, heat capacity and Raman spectra of Ba_2MgWO_6 single crystals grown in $BaCl_2$-$MgCl_2$ flux

Jana Pásztorová [a,*], Wen Hua Bi [b], Richard Gaal [a], Karl Krämer [c], Ivica Živković [a], Henrik M. Rønnow [a]

[a] Laboratory for Quantum Magnetism, Institute of Physics, École Polytechnique Fédérale de Lausanne, CH-1015 Lausanne, Switzerland
[b] Crystal Growth Facility, École Polytechnique Fédérale de Lausanne, CH-1015 Lausanne, Switzerland
[c] Department of Chemistry, Biochemistry and Pharmacy, University of Bern, CH-3012 Bern, Switzerland

A B S T R A C T

We present a new method of Ba_2MgWO_6 single crystal synthesis that allows to grow larger crystals using a $BaCl_2$ and $MgCl_2$ flux. Difficulties to grow single crystals of a size suitable for macroscopic material property measurements caused the majority of characterisation being published on polycrystalline samples. Our single crystal diffraction and energy dispersive X-ray analysis confirmed high quality of synthesised samples. Heat capacity measurements from 300 K to 2 K do not show any phase transitions. However, Raman spectra measured down to 77 K contain additional weak peaks at all temperatures probed, which is in a contrast with only 4 Raman active modes expected from the crystal structure with the space group $Fm\bar{3}m$. This calls for a more detailed study of potential symmetry breaking that could also influence the electronic properties of the material.

1. Introduction

Perovskites ABO_3, the parent compound crystallizing in the space group $Pm\bar{3}m$, were in a scope of scientific interest for a long time due to a vast variety of electronic, magnetic and optical properties [1,2]. In case of double perovskites $A_2BB'O_6$, also referred to as Elpasolites, the octahedral B site is now occupied by two different types of cations B and B', which naturally increases the variety of properties [3]; the lattice parameter is doubled and space group changes to $Fm\bar{3}m$. Tungsten in its typical oxidation state 6+, is an ideal candidate to occupy the B' site in $A_2BB'O_6$, creating a bond with 6 oxygen atoms in the octahedral fashion. The early studies on A_2BWO_6 [4–6], mostly on polycrystalline samples, established structural properties and octahedral distortion. However, the presence of another phase in the polycrystalline samples often prevented the further analysis of intrinsic properties of A_2BWO_6 [7]. The distortion is particularly important when assessing electric properties of a material, as the octahedral tilting can break inversion symmetry which is critical for ferroelectricity. This links to studies which tried to determine the potential of tungstates as ceramic materials for microwave applications [8,9].

To the best of our knowledge, there is only one publication on the single crystal growth of Ba_2MgWO_6 in a K_2CO_3 flux [10]. No single crystal measurements of material properties have been reported to date.

In this paper, we will present the growth of larger sized Ba_2MgWO_6 single crystals obtained by a new route from oxides BaO, MgO and WO_3, in a halide flux of $BaCl_2$ and $MgCl_2$. The reaction in sealed Pt ampules eliminates the risk of potassium (K_2CO_3 flux) and aluminium (Al_2O_3 crucible) contamination. The idea was based on a successful growth of Ba_2MgReO_6 single crystals [11]. The ionic radius of non-magnetic W^{6+} ions is comparable to magnetic Re^{6+} ions. Finally, we report novel data for specific heat and Raman spectra measured on single crystals measured down to low temperatures.

2. Experimental procedure

2.1. Materials

The following chemicals were used for the synthesis: BaO (Sigma Aldrich, 99.99%), MgO (Apollo Scientific, 99.99%), WO_3 (Fluka, 99.9%), and $BaCl_2$ (ABCR Swiss AG, ultra dry, 99.998%), $MgCl_2$ (ABCR Swiss AG, ultra dry, 99.99%) as a flux.

2.2. Single crystal growth

BaO, MgO and WO_3 were mixed in stoichiometric ratios and ground thoroughly in an agate mortar in an Ar glove box to avoid moisture.

* Corresponding author.
E-mail address: pasztorovaj@gmail.com (J. Pásztorová).

https://doi.org/10.1016/j.jssc.2023.124184
Received 13 April 2023; Received in revised form 21 June 2023; Accepted 27 June 2023
Available online 7 July 2023

The flux composed of 71 wt% $BaCl_2$ and 29 wt% $MgCl_2$ was added and mixed thoroughly. The mixture with the total mass of 4 g (3 g of starting materials and 1 g of the flux) was then placed in a platinum tube of 95 mm length and 10 mm diameter and sealed by arc melting under a protective Ar atmosphere. The tube was heated to 1400 °C where it was kept for 15 h and then slowly cooled to 950 °C at a rate of 1.5 °C/h, followed by furnace cooling to room temperature. The excess flux was removed by washing with distilled water in an ultrasonic bath. Crystals were isolated by the vacuum filtration.

2.3. Scanning electron microscopy

The chemical composition of the single-crystalline Ba_2MgWO_6 samples was verified by energy dispersive X-ray spectroscopy in a scanning electron microscope (SEM-EDX, Zeiss GeminiSEM 300 with Oxford Instr. EDX detector) in high-vacuum mode. EDX spectroscopy confirmed the presence of Ba, Mg, W and their respective stoichiometric ratios within the elemental detection limits of the instrument.

2.4. Single crystal X-ray diffraction

The quality of the single crystals was checked using a Rigaku Synergy-I XtaLAB X-ray diffractometer, equipped with a Mo microfocusing source (λK_α = 0.71073 Å) and a HyPix-3000 Hybrid Pixel Array detector (Bantam). Data reduction, scaling and absorption corrections were performed using 1.171.41.119a (Rigaku OD, 2021). The final completeness is 100% out to 36.053° in θ. A multi-scan absorption correction was performed using *CrysAlisPro* 1.171.41.119a. The empirical absorption correction was done using spherical harmonics, implemented in *SCALE3 ABSPACK* scaling algorithm. The absorption coefficient μ of this crystal is 36.310 mm^{-1} (at λK_α = 0.71073 Å) and the minimum and maximum transmissions are 0.609 and 0.749.

The collected data were refined using *OLEX2* [12] and *ShelXL* software [13].

2.5. Heat capacity

Specific heat was measured by Quantum Design Physical Property Measurement System utilising the relaxation method.

2.6. Raman spectroscopy

Raman spectrum of Ba_2MgWO_6 single crystal was measured on a Horiba HR-800 spectrometer equipped with a 532 nm laser, a 600 l/mm grating and a Symphony II nitrogen cooled CCD detector. An Olympus objective with 50x magnification and long working distance was used. The sample was mounted on the cold finger of a Conti continuous flow cryostat. Spectra were taken every 50 K, from 300 K down to 100 K and at 77 K. Peaks were identified and fitted with a Pearson VII line shape.

3. Results and discussion

3.1. Preparation, elemental and structural analysis

The grown crystals have average size of 0.4 mm and the typical morphology of truncated octahedron as can be seen in Fig. 1. The maximum size was 0.6 mm (used for heat capacity measurement, Fig. 5). The growth had a high yield of crystals - for total mass of 4 g of starting materials and flux, the single crystal yield was 0.5 g. Crystals have semi-transparent light brown colour.

EDX spectra and element distribution maps were recorded from several selected crystals and from different facets on each of these single crystals. The elemental mapping (Fig. 2) demonstrates that the Ba, Mg, W and O atoms are uniformly distributed on the surface of tested single crystals within the detection limit of the technique. The image resolution was 1024 x 768 pixels with 135 400 counts per image.

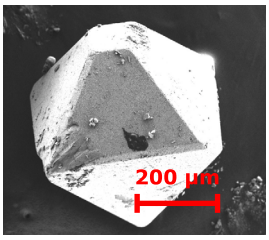

Fig. 1. SEM photograph of a typical Ba_2MgWO_6 single crystal with truncated octahedral shape.

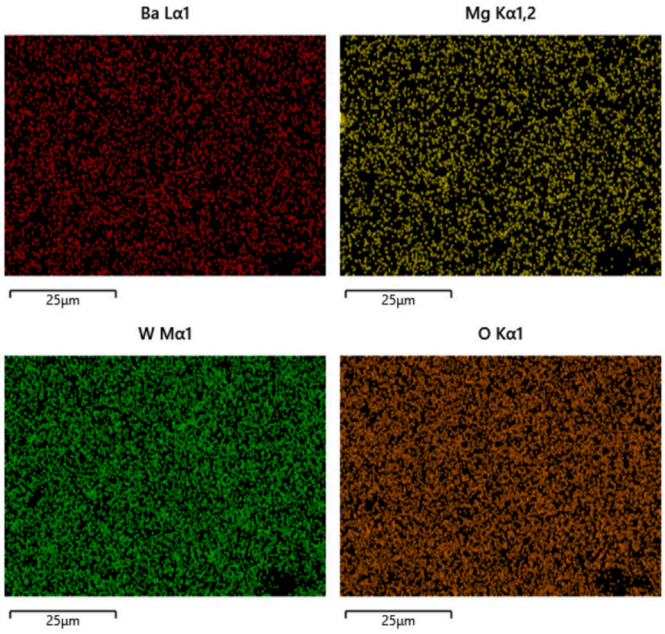

Fig. 2. Uniform distribution of Ba, W, Mg and O elements measured on Ba_2MgWO_6 single crystal.

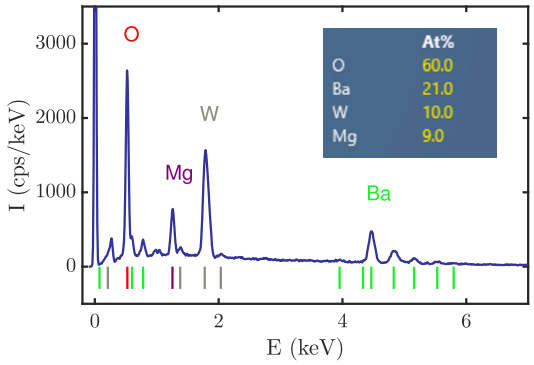

Fig. 3. EDX analysis of a Ba_2MgWO_6 single crystal. Vertical lines below the spectra indicate x-ray peaks of individual elements. For better reading, only major peaks are labeled. All peaks are explained by the four present elements. The results are consistent with data measured on other crystals and facets.

The molar ratio of Ba, Mg, W and O are determined to be very close to the stoichiometric Ba_2MgWO_6 sample (Fig. 3). The fit of peak position and intensity was performed automatically by Oxford Instr. EDX software. For the clarity of Fig. 3, only major peaks were labeled. Two small peaks at 0.601 and 0.780 keV were identified as a signal coming from the Ba element. All peaks are explained by four present elements. The software analysing the data defined mass percentage (wt %) of individual elements in the Ba_2MgWO_6 sample as following - 14.39%

Table 1
Structure refinement details from single crystal X-ray diffraction on Ba_2MgWO_6, using the wavelength $\lambda =$ 0.71073 Å and space group $Fm\bar{3}m$ at 100 K and 300 K.

	100 K	300 K
Formula weight	578.84	578.84
a (Å)	8.1010(2)	8.1120(3)
V (Å^3)	531.64(4)	533.81(6)
ρ_c (g cm^{-3})	7.232	7.203
μ (mm^{-1})	36.310	36.163
F(000)	984	984
Crystal size (mm)	0.04×0.03×0.02	0.01×0.07×0.03
Reflections collected	890	461
Independent reflections	95	64
R_{int}	0.0186	0.0136
Goodness of fit on F^2	1.088	1.137
R_1	0.0105	0.0122
wR_2	0.0251	0.0280
Largest diff. peak/hole (e Å^{-3})	0.698 and -0.555	1.090 and -0.642

Table 2
Atomic sites, positions and equivalent isotropic displacement parameters for Ba_2MgWO_6 at 100 K. U_{eq} is defined as one third of the trace of the orthogonalized U_{ij} tensor.

Atom	Site	x	y	z	U_{ij} (Å^2)
Ba	8c	0.25	0.25	-0.25	0.003(1)
Mg	4a	0	0	0	0.003(1)
W	4b	0	0	-0.5	0.002(1)
O	24e	0	0	-0.2384(4)	0.004(1)

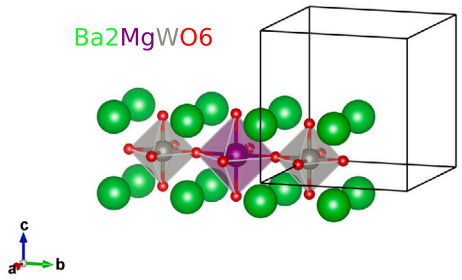

Fig. 4. The crystal structure of Ba_2MgWO_6. The cubic unit cell and W-O_6 and Mg-O_6 octahedra are visualised in VESTA software.

oxygen, 49.83% barium, 31.94% tungsten and 3.84% for magnesium. That translates into - 56.43%, 22.76%, 10.90% and 9.91% atomic percentages (at %). The standard deviation σ wt % was 0.29%, 0.69%, 0.60% and 0.14%, respectively.

Single crystal X-ray diffraction was performed on a representative crystal at 300 K and 100 K. According to the results of data reduction with *CrysAlisPro* program, all diffraction spots can be indexed by the F-centered cubic unit cell. The lattice parameters for $Fm\bar{3}m$ space group, collection details and refinement information are given in Tables 1 and 2. Results are consistent with previous work [10]. Ba_2MgWO_6 adopts the cubic double perovskite structure with alternating, corner shared octahedra of MgO_6 and WO_6, with Ba cations occupying spaces in between, see Fig. 4.

The bond lengths refined from the single crystal X-ray diffraction data at room temperature are following - Ba-O 2.86991(17) Å, Mg-O 2.132(4) Å and W-O 1.924(4) Å. The bonds become slightly shorter at 100 K - Ba-O 2.86568(12) Å, Mg-O 2.119(3) Å and W-O 1.931(3) Å. The x-ray analysis on Ba_2MgWO_6 polycrystalline sample ($T = 300$ K) published in the article [10] established interatomic distances as following - Ba-O 2.8679(4) Å, Mg-O 2.145(4) Å and W-O as 1.907(4) Å. In fact, our new single crystal diffraction data are in better agreement with values of the neutron powder diffraction refinement at room temperature [10]. When comparing to Ba_2MgReO_6 x-ray data collected at room temperature, the interatomic Ba-O distance is rather similar. Larger differences occur for - Mg-O 2.082(4) Å and Re-O 1.961(4) Å [14], respectively.

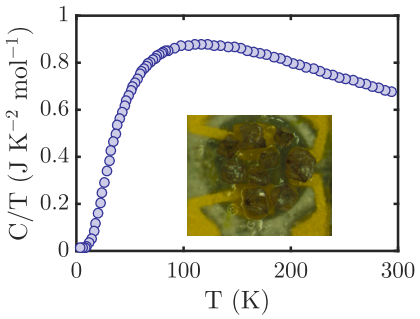

Fig. 5. Temperature dependence of specific heat divided by temperature C/T measured on Ba_2MgWO_6 single crystals. The data show no anomaly in the temperature range from 300 K to 2 K. The inset shows single crystals on the PPMS puck platform with dimensions 3×3 mm.

We also examined the possibility of Mg/W site mixing which may occur in a case of double perovskites. For the W site (4b), we refined an occupancy factor equal to 0.995(19) which excludes Mg atoms on this site. The occupation factor for the Mg site (4a) was refined to 0.959(15), excluding any heavy element occupying it. We will refer to this result in the chapter about Raman spectra.

3.2. Heat capacity

Specific heat measurements used a sample puck with integrated heater and thermometer. Before mounting Ba_2MgWO_6 crystals on the platform, a background measurement was performed with a small amount of the apiezon N grease. Subsequently, 9 octahedrally shaped crystals with a total mass of 3.6 mg were placed with the {111} facet parallel to the puck. In Fig. 5, we show measured specific heat divided by temperature C/T for the temperature range from 300 K to 2 K in zero magnetic field. The specific heat follows the typical shape for phononic heat of an insulator and no indication of a phase transition induced anomaly was observed.

3.3. Raman spectroscopy

The allowed number of Raman active vibrational modes can be deduced from the site symmetry of the atomic positions and the space group [15]. The face centered cubic Ba_2MgWO_6 double perovskite with space group $Fm\bar{3}m$ has four atomic sites (see Table 4) resulting in following mechanical representation:

$$M = A_{1g} + E_g + F_{2u} + 2F_{2g} + 5F_{1u} + F_{1g},$$

that can be broken down into acoustic and optic modes:

$$\Gamma_{acoustic} = F_{1u},$$

$$\Gamma_{optic} = A_{1g} + E_g + F_{2u} + 2F_{2g} + 4F_{1u} + F_{1g},$$

where F_{1g}, F_{2u} are silent optic modes. A denotes the non-degenerate mode, E and F denote double- and triple-degenerate modes, respectively. The symmetry analysis predicts only 4 Raman active modes that appear at different frequencies in the vibration spectrum:

$$\Gamma_{Ram} = A_{1g} + E_g + 2F_{2g}.$$

Raman spectra collected from 300 K down to 77 K on a Ba_2MgWO_6 single crystal are shown in Fig. 6. The spectra contain three strong and a few weak Raman modes for all temperatures. Our single crystal data show a very good agreement with those from the ceramic material by Diao et al. [8], i.e. - the three strong $F_{2g}(1)$, $F_{2g}(2)$, A_g modes and one weak E_g mode. The energies of those four measured modes are also

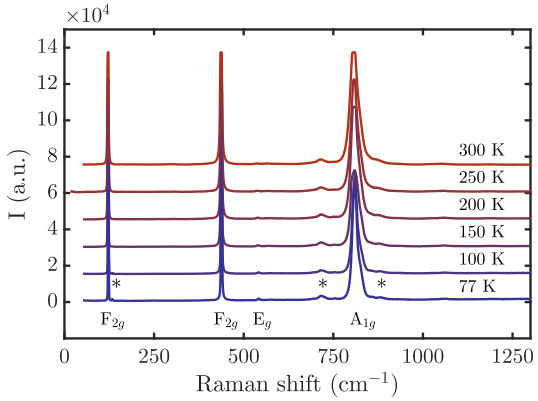

Fig. 6. Temperature dependence of Raman spectra measured on Ba_2MgWO_6 single crystals. Four expected Raman modes for space group $Fm\bar{3}m$ are indicated under the data sets, additional peaks are marked with asterisks at 130, 716 and 880 cm^{-1}.

Table 3
First column represents experimentally defined Raman modes at 300 K in this study (†). Following columns show the comparison with experimental data at 300 K on the ceramic material [8], and two theoretical calculations of phonon spectra [8,16].

R. mod.	ν (cm^{-1})			
	exp(†)	exp [8]	DFT [8]	LDC [16]
$F_{2g}(1)$	123	126	105	125
$F_{2g}(2)$	439	441	405	432
$E_g(1)$	536	538	614	522
$A_{1g}(1)$	807	812	833	776

in reasonable agreement with phonon spectrum calculations utilising density functional theory (DFT) [8] and lattice dynamic calculations (LDC) [16]. These results are summarized in Table 3. However, the data show some notable differences. The improved signal to noise ratio in our data allows the observation of more subtle peaks in the spectra. These can not be explained by the initial analysis for space group $Fm\bar{3}m$. Three additional peaks have Raman shift of 130, 716 and 880 cm^{-1} (values were obtained from the fit of 77 K data set) and are marked with asterisks in Fig. 6. The additional mode at 130 cm^{-1} increases in amplitude upon cooling.

The closer inspection of A_{1g} mode revealed that it could not be fit by a single Pearson VII line shape due to the peak's tail at higher frequencies. The width of this mode is reduced with decreasing temperature, uncovering a new vibration very close to the 812 cm^{-1} Raman shift established in [8]. Two peaks at 300 K and three peaks with Pearson VII line shape at 77 K were needed to fit its shape and are plot in the inset of Fig. 7.

Raman scattering has advantages over diffraction techniques, mainly because of its sensitivity to detect local disorder and symmetry lowering. From the many possible reasons why additional bands may appear in Raman spectra, some are easily eliminated due to the character of Ba_2MgWO_6 compound. The electronic configuration of W^{6+} is $5d^0$, therefore Ba_2MgWO_6 is non-magnetic and should have no contribution from magnons. The structural analysis confirmed that there is no Mg/W site mixing. This is also prevented by the fact that the oxidation states of Mg and W ions differ by 4. Therefore, the most likely scenario of additional bands comes from local symmetry lowering, which might be due to positional disorder or defects. Slight departure from proposed $Fm\bar{3}m$ space group (on average or locally) can alter the operations of symmetry. The distortion of an ideal octahedron was observed in other double perovskite materials such as Ba_2MgReO_6 [17,18] and it is a tendency indicated in past studies as well [4]. Multiple areas and

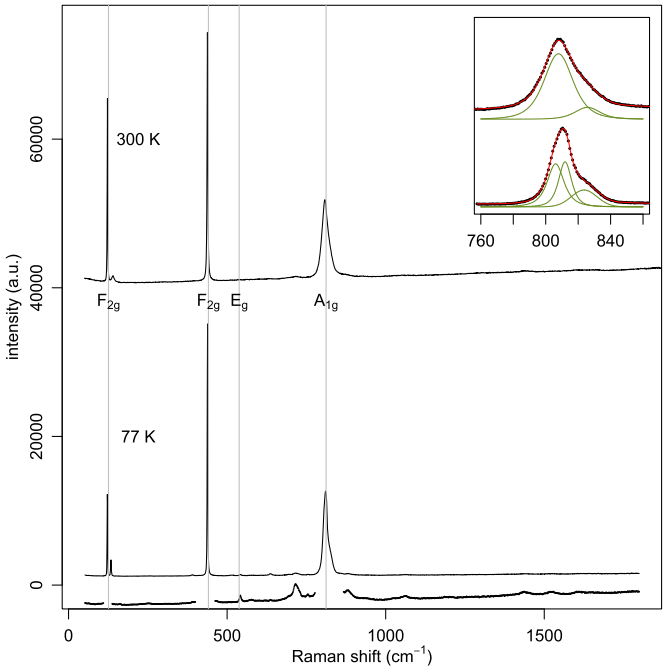

Fig. 7. Raman spectra of Ba_2MgWO_6 single crystal at 300 and 77 K. Grey vertical lines mark the position of the 4 Raman active modes found by Diao et al. [8]. Data depict splitting of lower $F_{2g}(1)$ mode, weak E_g mode and asymmetric peak of A_{1g} Raman shift. The inset shows close up on A_{1g} mode that can not be characterised by a single Pearson function, even at room temperature. Two components are necessary for data set at 300 K and three for 77 K data. Red line is the fit including a smooth baseline, green the individual components.

Table 4
The atomic site group analysis of active Raman modes in ordered Ba_2MgWO_6 double perovskites [15]. A_{1g} and E_g Raman modes correspond to oxygen vibrations only, whereas Mg and W atoms do not contribute to active Raman modes.

Atom	Site	Active Ram. modes
Ba	8*c*	F_{2g}
Mg	4*a*	-
W	4*b*	-
O	24*e*	A_{1g} + E_g + F_{2g}

different spots were measured with the same consistent results, which points towards an intrinsic property of a material, rather than defects.

From the atomic site group analysis of active Raman modes (see Table 4), it is possible to see that W and Mg atoms do not have active phonon contribution in the Raman spectra. The A_{1g} Raman active mode represents symmetric stretching of oxygen atoms only, along Mg-O-W axis, describing breathing-type vibrations of the octahedra. The extra modes appearing around A_{1g} might be coming from local symmetry lowering. The E_g mode corresponds to asymmetric stretching of oxygen bonds. The lowest frequency F_{2g} mode is linked with translations of the Ba cation [5].

4. Conclusion

Single crystals of the cubic double perovskite Ba_2MgWO_6 have been grown by a new method using $BaCl_2$ and $MgCl_2$ flux. Obtained crystals have the average size of 0.4 mm with largest crystals up to 0.6 mm, thus providing an opportunity for material property investigations on single crystals. Heat capacity measurements show no phase transitions from 2 K to 300 K for this compound. The temperature dependence of Raman spectra revealed additional minor modes that are not consistent with four exclusive Raman active modes established for $Fm\bar{3}m$ space

group. For better understanding of Ba_2MgWO_6 Raman spectra, more measurements are needed, especially, at $T < 77$ K, to clarify the true symmetry of the compound. The symmetry analysis is also important in the context of ferroelectric properties and potential practical applications of Ba_2MgWO_6.

CRediT authorship contribution statement

Jana Pásztorová: Data curation, Formal analysis, Investigation, Validation, Visualization, Writing – original draft, Writing – review & editing. **Wen Hua Bi:** Formal analysis, Investigation, Validation. **Richard Gaal:** Formal analysis, Investigation, Validation. **Karl Krämer:** Supervision, Writing – review & editing. **Ivica Živković:** Methodology, Supervision, Writing – review & editing. **Henrik M. Rønnow:** Funding acquisition, Methodology, Resources, Supervision, Writing – review & editing.

Declaration of competing interest

The authors declare that they have no known competing financial interests or personal relationships that could have appeared to influence the work reported in this paper.

Data availability

Data will be made available on request.

Acknowledgement

This work was funded by the European Research Council (ERC) under the European Union's Horizon 2020 research and innovation program projects HERO (Grant No. 810451). We thank the Interdisciplinary Centre for Electron Microscopy at EPFL (CIME), K. Krämer and Daniel Biner at University of Bern for initial growths, and Jens Kreisel for insightful discussions about Raman spectra.

References

[1] F.S. Galasso, Structure, Properties and Preparation of Perovskites, 1st ed., Pergamon Press, Oxford, 1969.

[2] G. Shirane, H. Danner, R. Pepinsky, Neutron diffraction study of $BaTiO_3$, Phys. Rev. 105 (1957) 856.

[3] W.-J. Yin, B. Weng, J. Ge, Q. Sun, Z. Li, Y. Yan, Oxide perovskites, double perovskites and derivatives for electrocatalysis, photocatalysis, and photovoltaics, Energy Environ. Sci. 12 (2019) 442.

[4] E.G. Steward, H.P. Rooksby, Pseudo-cubic alkaline-earth tungstates and molybdates of the R_2MX_6 type, Acta Crystallogr. 4 (1951) 503.

[5] M. Liegeois-Duyckaerts, P. Tarte, Vibrational studies of molybdates, tungstates and related compounds-III. Ordered cubic perovskites $A_2B^{II}B^{VI}O_6$, Spectrochim. Acta 30 (1974) 1771–1786.

[6] B.E. Day, N.D. Bley, H.R. Jones, R.M. McCullough, H.W. Eng, S.H. Porter, P.M. Woodward, P.W. Barnes, Structures of ordered tungsten- or molybdenum-containing quaternary perovskite oxides, J. Solid State Chem. 185 (2012) 107.

[7] R.L. Andrews, A.M. Heyns, P.M. Woodward, Raman studies of A_2MWO_6 tungstate double perovskites, Dalton Trans. 44 (2015) 10700.

[8] C.-L. Diao, C.-H. Wang, N.-N. Luo, Z.-M. Qi, T. Shao, Y.-Y. Wang, J. Lu, F. Shi, X.-P. Jing, First-principle calculation and assignment for vibrational spectra of $Ba(Mg_{1/2}W_{1/2})O_3$ microwave dielectric ceramic, J. Am. Ceram. Soc. 96 (2013) 2898.

[9] D.D. Khalyavin, J. Han, A.M.R. Senos, P.Q. Mantas, Synthesis and dielectric properties of tungsten-based complex perovskites, J. Mater. Res. 18 (2003) 2600–2607.

[10] D.E. Bugaris, J.P. Hodges, A. Huq, H.-C. zur Loye, Crystal growth, structures, and optical properties of the cubic double perovskites Ba_2MgWO_6 and Ba_2ZnWO_6, J. Solid State Chem. 184 (2011) 2293.

[11] D. Hirai, Z. Hiroi, Successive symmetry breaking in a $J_{eff} = 3/2$ quartet in the spin–orbit coupled insulator Ba_2MgReO_6, J. Phys. Soc. Jpn. 88 (2019) 064712.

[12] O.V. Dolomanov, L.J. Bourhis, R.J. Gildea, J.A.K. Howard, H. Puschmann, OLEX2: a complete structure solution, refinement and analysis program, J. Appl. Crystallogr. 42 (2009) 339.

[13] G.M. Sheldrick, Crystal structure refinement with SHELXL, Acta Crystallogr., Sect. C 71 (2015) 3.

[14] K. Bramnik, H. Ehrenberg, J. Dehn, H. Fuess, Preparation, crystal structure, and magnetic properties of double perovskites M_2MgReO_6 (M: Ca, Sr, Ba), Solid State Sci. 5 (2003) 235.

[15] E. Kroumova, M.I. Aroyo, J.M. Perez-Mato, A. Kirov, C. Capillas, S. Ivantchev, H. Wondratschek, Bilbao crystallographic server: useful databases and tools for phase-transition studies, Phase Transit. 76 (2003) 155.

[16] J. Rodrigues, D. Bezerra, A. Hernandes, Calculation of the optical phonons in ordered Ba_2MgWO_6 perovskite using short-range force field model, J. Raman Spectrosc. 49 (2018) 1822.

[17] D. Hirai, H. Sagayama, S. Gao, H. Ohsumi, G. Chen, T.-h. Arima, Z. Hiroi, Detection of multipolar orders in the spin-orbit-coupled $5d$ Mott insulator Ba_2MgReO_6, Phys. Rev. Res. 2 (2020) 022063.

[18] J. Pásztorová, A.M. Tehrani, I. Živković, N.A. Spaldin, H.M. Rønnow, Experimental and theoretical thermodynamic studies in Ba_2MgReO_6—the ground state in the context of Jahn-Teller effect, J. Phys. Condens. Matter 35 (2023) 245603.